Simplified Method to Quantify Valve Back-leak Uncovers Severe Mesenteric Lymphatic Valve Dysfunction in Mice Deficient in Connexins 43 and 37

Jorge A. Castorena-Gonzalez[1], R. Sathish Srinivasan[2], Philip D. King[3], Alexander M. Simon[4], and Michael J. Davis[1]

[1]*Department of Medical Pharmacology and Physiology, School of Medicine, University of Missouri, Columbia, MO, USA*
[2]*Cardiovascular Biology Research Program, Oklahoma Medical Research Foundation, Oklahoma City, OK, USA*
[3]*Department of Microbiology and Immunology, University of Michigan Medical School, Ann Arbor, MI, USA*
[4]*Department of Physiology, University of Arizona, Tucson, AZ, USA*

Running Title: Simplified Method Uncovers Severe Lymphatic Valve Dysfunction

Key Points Summary:

- Lymphatic valve defects are one of the major causes of lymph transport dysfunction; however, there are no accessible methods for quantitatively assessing valve function.
- This manuscript provides a novel technique for quantifying lymphatic valve back-leak.
- Postnatal endothelial-specific deletion of Cx43 in $Cx37^{-/-}$ mice results in rapid regression of valve leaflets and severe valve dysfunction.
- This method can also be used for assessing the function of lymphatic valves from various species, including humans.

ABSTRACT

The lymphatic system relies on robust, spontaneous contractions of collecting lymphatic vessels and one-way secondary lymphatic valves to efficiently move lymph forward. Secondary valves prevent reflux and allow for the generation of propulsive pressure during each contraction cycle. Lymphatic valve defects are one of the major causes of lymph transport dysfunction. Genetic mutations in multiple genes have been associated with the development of primary lymphedema in humans and many of the same mutations in mice result in valve defects that subsequently lead to chylous ascites or chylothorax. At present the only experimental technique for the quantitative assessment of lymphatic valve function utilizes the servo-null micropressure system, which is highly accurate and precise, but relatively inaccessible and difficult to use. We developed a novel, simplified alternative method for quantifying valve function and determining the degree of pressure back-leak through an intact valve in pressurized, single-valve segments of isolated lymphatic vessels. With this diameter-based method, the competence of each lymphatic valve is challenged over a physiological range of pressures (e.g. 0.5-10 cmH_2O) and pressure back-leak is extrapolated from calibrated, pressure-driven changes in diameter upstream from the valve. Using mesenteric lymphatic vessels from *C57BL/6J*, *Ub-CreER^{T2};Rasa1$^{fx/fx}$*, *Foxc2$^{+/-}$*, *Lyve1-Cre*;$Cx43^{fx/fx}$, and *Prox1-CreER^{T2}*;$Cx43^{fx/fx}$;$Cx37^{-/-}$ mice, we tested our method on lymphatic valves displaying a wide range of dysfunction, from fully-competent to completely incompetent. Our results were validated by simultaneous direct measurement of pressure

This is an Accepted Article that has been peer-reviewed and approved for publication in the The Journal of Physiology, but has yet to undergo copy-editing and proof correction. Please cite this article as an 'Accepted Article'; doi: 10.1113/JP279472.

back-leak using a servo-null micropressure system. Our diameter-based technique can be used to quantify valve function in isolated lymphatic valves from a variety of species.

Keywords: Lymphatic vessel, back-leak, valve function, servo-null micropressure system, lymph transport, Connexin37, Connexin43, Foxc2, Rasa1

INTRODUCTION

Secondary lymphatic valves are located throughout networks of collecting lymphatic vessels and function to facilitate unidirectional movement of lymph centrally toward the great veins. Functional lymphatic valves are critical in preventing back flow in the face of a gravitational load, but also in supine body positions because even then lymph is transported against a slight adverse pressure gradient (Hargens & Zweifach, 1976). Multiple genetic mutations including *FOXC2, RASA1, and PIEZO1* lead to human primary lymphedema as a result of lymphatic valve defects, as revealed by murine models recapitulating the human gene defects (Sabine *et al.*, 2015; Lapinski *et al.*, 2017; Nonomura *et al.*, 2018).

Quantitative measurements of lymphatic valve function in mice are invaluable in distinguishing the cause of lymphatic transport dysfunction, which can potentially be caused by a number of factors, including contractile dysfunction (Castorena-Gonzalez *et al.*, 2018b), defective lymphangiogenesis (Karkkainen *et al.*, 2000), and/or abnormal valves (Sabine *et al.*, 2015; Lapinski *et al.*, 2017; Nonomura *et al.*, 2018). In vivo observations of back flow in lymphatic networks, e.g. using tracers, can be indicators of valve dysfunction but may also be misleading because a brief period of back flow occurs normally during the lymphatic contraction cycle and because lymphatic valves are biased to be open when the trans-valve pressure gradient is zero or even fractionally adverse (Davis *et al.*, 2011a). Likewise, more sophisticated in vivo methods such as optical coherence tomography, which can provide information about valve dynamics (Blatter *et al.*, 2018) if a valve is properly orientated, cannot provide quantitative information about back-leak or valve stiffness in the absence of pressure measurement/control. Without pressure information, the complicated relationship between vessel diameter and the pressure difference required for valve closure (Davis *et al.*, 2011b; Scallan *et al.*, 2013; Lapinski *et al.*, 2017) can lead to a misinterpretation of valve function.

We previously devised two ex vivo tests for quantifying normal and abnormal valve function in rat and mouse collecting lymphatic vessels (Davis *et al.*, 2011a; Lapinski *et al.*, 2017). A vessel segment containing a single valve is cannulated at each end (requiring ~40 μm-tip micropipettes in mouse vessels) and, using independent pressure control at each end, valve behavior is observed under an inverted microscope. 1) In the first method, the adverse pressure required to close an open valve is tested in response to a ramp-wise increase in outflow pressure while inflow pressure is held constant (Davis *et al.*, 2011a); this test provides information about the material properties of the valve (e.g. stiffness), which may change if critical valve leaflet components are deleted. Normal mouse and rat valves require from 0.1 to ~3 cmH_2O adverse pressure gradient to close, while defective valves may require >30 cmH_2O or never close. 2) In the second method, pressure back-leak through a closed valve is measured by inserting a sharpened servo-nulling micropipette (~3-5 μm tip) through the vessel wall into the lumen upstream from the valve while the valve is challenged by elevation of outflow pressure (Sabine *et al.*, 2015; Lapinski *et al.*, 2017); the degree of pressure back-leak is a measure of valve competency, i.e. how well the leaflets seal. A servo-null micropipette measurement (Wiederhielm *et al.*, 1964) is needed to detect changes in lumenal pressure behind the closed valve because the amount of back flow (nL/min) is typically too small to be detected through the cannulating pipette by an upstream pressure transducer.

Normal mouse valves show little or no pressure back-leak in the latter test, whereas defective valves (*Foxc2*-, *Rasa1*-, *Gja1*-, *Gata2*-deficient) show a range of back-leak from

mild (Munger *et al.*, 2017; Cha *et al.*, 2018) to severe (Sabine *et al.*, 2015; Lapinski *et al.*, 2017). It is anticipated that mutations or deficiencies in other genes (including those coding for *Gja4*, *Gjc2* and other junctional proteins between lymphatic endothelial cells (LECs) may lead to varying degrees of lymphatic valve back-leak that can only be quantified by the back-leak test. However, servo-null micropressure systems are no longer available commercially, are difficult to use, and require extensive training for proper use and calibration, making that method inaccessible to most laboratories. For this reason, we devised a method for quantifying valve back-leak that does not require a servo-nulling micropressure system. Comparison of this novel, diameter-based method with the servo-null method in a large set of normal and defective mouse mesenteric lymphatic valves gave excellent agreement over a range of adverse pressure gradients (0.5 to 5 cmH_2O, spanning the presumed physiological range (Castorena-Gonzalez *et al.*, 2018b)), allowing quantitative measurement of valve back-leak in a cannulated lymphatic vessel from a simple diameter measurement.

METHODS

Study Approval. All animal protocols and procedures were approved by the University of Missouri Animal Care and Use Committee and conformed to the US Public Health Service policy for the humane care and use of laboratory animals (PHS Policy, 2011).

Mice. Both female and male mice were used for the experiments included in these studies. Mice were housed in groups of 2-4 mice per cage at a temperature of 22-25^{o}C under a 12-hour light/dark cycle. Mice had access to food (PicoLab RodentDiet 20 Cat. No. 355043) and water at all times. Mice were anesthetized by intraperitoneal injection of Ketamine/Xylazine (0.1 mL/25 g) and placed on a heated tissue dissection/isolation pad. To ensure adequate anesthesia level prior and during dissection, indicators of pain were continuously monitored by assessing loss of pedal and pinna reflexes. At the end of the dissection, animals were euthanized via intracardiac KCl injection. Data were collected from the following mouse lines: *WT* (*C57BL/6J* purchased from The Jackson Laboratory – Bar Harbor, MA, USA), *Ub-CreER^{T2};Rasa1$^{fx/fx}$* (obtained from Philip D. King, University of Michigan), *Foxc2-Cre* (obtained from Sathish Srinivasan, OMRF), *Lyve1-Cre;Cx43$^{fx/fx}$*, *Prox1-CreER^{T2};Cx43$^{fx/fx}$;Cx37$^{-/-}$* mice generated in house by crossing *Cx37$^{-/-}$*, *Cx43$^{fx/fx}$* mice (Simon *et al.*, 1997; Liao *et al.*, 2001) and *Prox1-CreER^{T2}* mice. *Prox1-CreER^{T2}* mice were obtained from Taija Mäkinen, University of Uppsula, Sweden. *Prox1-CreER^{T2};Cx43$^{fx/fx}$;Cx37$^{-/-}$* mice were induced via feeding tamoxifen-containing chow (ENVIGO TD.130855) for one week (~40 mg/kg of body weight per day assuming a 20-25 g body weight and a 3-4 g intake); and experiments were conducted 5-7 days post-induction. *Ub-CreER^{T2};Rasa1$^{fx/fx}$* mice were studied 4-5 months post-induction.

Vessel Isolation, Pressure Myography, and Data Acquisition. Mesenteric lymphatic vessels were isolated as previously described (Scallan & Davis, 2013; Scallan *et al.*, 2016; Zawieja *et al.*, 2017; Castorena-Gonzalez *et al.*, 2018a; Castorena-Gonzalez *et al.*, 2018b; Zawieja *et al.*, 2018). Each vessel was pinned down with short segments of 40 µm stainless steel wire onto the Sylgard-coated surface of a dissection chamber filled with BSA containing Krebs buffer at room temperature. The large majority of the adipose and connective tissues surrounding the lymphatic vessels were cleared by micro-dissection. The vessel was then transferred to a 3-mL observation chamber containing BSA containing Krebs buffer, cannulated, and pressurized to 3 cmH_2O, under no-flow conditions, using two glass micropipettes. For all experiments used in this study, we used the same pair of inflow and outflow pipettes, maintaining their orientation; inside diameter for each was ~40 µm. Micropipettes were mounted onto the micro-manipulator arm pipette holders of a Burg-style V-track pipette system. To ensure accurate diameter tracking, the cannulated vessel segment was further cleared of remaining connective and adipose tissue. Lymphatic segments contained a single valve. The pipette system with cannulated lymphatic vessel segment was transferred onto the XY-stage of an inverted microscope for observation. Polyethylene tubing was attached to the back of each glass micropipette and then connected

to a microfluidic flow control system (Elveflow OB1 MK3, Paris) with attached low-pressure transducers. To minimize longitudinal bowing and associated diameter-tracking artifacts at higher intraluminal pressures, input (P_{in}) and output (P_{out}) pressures were briefly set to 10 cmH_2O at the beginning of every experiment, and the vessel segment was stretched axially to remove longitudinal slack. The vessel was then allowed to equilibrate at 37°C for 20-30 minutes in a Ca^{2+}-free Krebs buffer while both input and output pressures were set to 3 cmH_2O. Constant perfusion with Ca^{2+}-free Krebs buffer was maintained using a peristaltic pump at a rate of 0.5 mL/min. Custom-written LabVIEW programs (National Instruments; Austin, TX) acquired real-time analog data and digital video and detected the inner and outer diameter of the vessel (Davis *et al.*, 2006). Videos were recorded for further analyses in brightfield mode at 30 fps using a Basler acA2000-340km camera.

Solutions and Chemicals. Krebs buffer contained: 146.9 mM NaCl, 4.7 mM KCl, 2 mM $CaCl_2 \cdot 2H_2O$, 1.2 mM $MgSO_4$, 1.2 mM $NaH_2PO_4 \cdot H_2O$, 3 mM $NaHCO_3$, 1.5 mM Na-HEPES, and 5 mM D-glucose (pH = 7.4). An identical buffer was prepared with the addition of 0.5% bovine serum albumin (BSA). During cannulation Krebs -BSA buffer was present both luminally and abluminally; however, during the experiment the abluminal solution was exchanged with Ca^{2+}-free Krebs buffer (in which 3 mM EGTA replaced calcium). All chemicals were obtained from Sigma-Aldrich (St. Louis, MO), with the exception of BSA (US Biochemicals; Cleveland, OH), $MgSO_4$ and Na-HEPES (ThermoFisher Scientific; Pittsburgh, PA).

Servo-Null Micropressure System. In single-valve lymphatic segments superfused with Ca^{2+}-free Krebs buffer to prevent spontaneous contractions, intraluminal pressure was directly measured using a servo-null micro-pressure system, as described in detail previously (Sabine *et al.*, 2018). Briefly, servo-null micropipettes (~2 µm tip diameter) were pulled from borosilicate glass (1.0/0.5 mm outer diameter/inner diameter, Omega-dot; Frederick Haer, Bowdoin, ME) using a Sutter P-97 puller (Sutter Instrument, Novato, CA). The pipettes were back-filled with 2 M NaCl and connected to a servo-null micropressure system (model 4A; IPM, La Mesa, CA) to monitor intraluminal pressure in the input side of the lymphatic segment (upstream from the valve being tested). After the vessel was allowed to equilibrate in Ca^{2+}-free Krebs buffer at 37°C, the servo-null system was zeroed with the micropipette positioned just outside the vessel wall, the luminal pressure was briefly set to 10 cmH_2O and the vessel was impaled on the inflow side of the valve with a servo-null micropipette, positioned via a Narishige MO-102 micromanipulator (Lapinski *et al.*, 2017). A small hole was first made with a tapered pilot pipette before inserting the servo-null pipette. Successful micropuncture left the servo-null pipette tip free from obstruction in the vessel lumen. The servo-null calibration was checked and adjusted, if needed, by briefly raising P_{in} and P_{out} to 10 cmH_2O.

Identification of Appropriate Diameter Measurement Sites from Space Time Maps (STMs). Brightfield videos of the single-valve lymphatic segments during back-leak tests were analyzed to generate 2-dimensional maps (STMs) representing the measurement of the outside diameter (encoded in 8-bit grayscale and displayed using a colored LUT) over time (horizontal axis) at every position along the vessel (vertical axis). To measure the outside diameter over time along the entire vessel segment, 30-fps bright-field videos were processed frame by frame; a threshold was dynamically applied to each frame and the lymphatic walls were then detected via contour detection. Edge detection of the identified walls allowed determination of the distance between the outside edges of the lymphatic wall at each specific position along the longitudinal axis. Colored maps were created from 8-bit grayscale maps using the Physics LUT from ImageJ where blue and red colors represent the minimum and maximum detected diameters respectively. All video processing and 2-dimensional analyses were performed using a set of custom-written Python-based programs. These analysis tools were developed from previously published methods for GI

studies (Hennig *et al.*, 2010; Hennig *et al.*, 2015; Hennig, 2016) and recently adapted for lymphatic vessel studies (Castorena-Gonzalez *et al.*, 2018b).

Calculated Parameters. For a given *k-th* pressure, the cross-sectional distensibility (D_{CS}) is calculated as previously described (Foote *et al.*, 2016):

$D_{CS}=\Delta CSA/(CSA_i \times \Delta P)$,

where CSA is the cross-sectional area of the lymphatic vessel, $\Delta CSA=CSA_k-CSA_i$, and $\Delta P=P_k-P_i$. The *i-th* index points to the initial, baseline state (i.e. under 0.5 cmH_2O of intraluminal pressure).

Back-leak of pressure through a given valve was assessed when each valve was challenged with an output pressure of 5 cmH_2O while input pressure was set at 0.5 cmH_2O. Therefore, pressure back-leak was referenced to this initial input pressure (i.e. back-leak is the difference from the 0.5 cmH_2O baseline).

The accuracy of each measurement of pressure back-leak was determined by calculating the difference between the gold-standard servo-null method and the diameter-based method, and defined as:

$Error = |P_{Back\text{-}leak,Servo\text{-}Null}-P_{Back\text{-}leak,Diameter\text{-}Based}|$,

the accuracy was then calculated as:

$\%\ Accuracy = (Error/\ P_{Back\text{-}leak,Servo\text{-}Null}) \times 100\%$.

The precision of a given back-leak calculation is directly associated with the calculated standard-deviation of repeated, consecutive measurements of pressure back-leak for a given lymphatic valve.

STATISTICS

The number *n* refers to the total number of experiments (i.e. single-valve lymphatic segments) included in this study. In most cases, more than one lymphatic segment from the same mouse was successfully studied. Statistical significance between groups was assessed via two-Way ANOVA with correction for multiple comparisons using Dunnett's test. Results are reported as mean ± standard deviation with significance set at $p<0.05$. Correlation between measurements obtained with servo-null and the diameter-based method here described was determined via analysis of linear correlation (2-tailed, 95% confidence interval). The Pearson's correlation coefficient (*r*) is reported for the entire data set (i.e. $n=41$). All statistical analyzes were performed using GraphPad Prism 8.

RESULTS

Characterization of Pressure-Driven Diameter Changes in Single Valve Lymphatic Segments

Single-valve lymphatic vessel segments were cannulated and pressurized as described above at 37°C in Ca^{2+}-free Krebs (Figure 1A). Each lymphatic vessel was allowed to equilibrate under no flow conditions ($P_{in}=P_{out}$) at an intraluminal pressure of 3 cmH_2O while perfused with a Ca^{2+}-free Krebs solution and warmed up to 37°C for 20-30 minutes. After impalement and positioning of a servo-null micropipette, intraluminal pressure then was set to 0.5 cmH_2O and vessel diameter was allowed to reach a steady level. Pressure ramps were generated by simultaneously increasing P_{in} and P_{out} from 0.5 to 10 cmH_2O (Figure 1B). Changes in diameter were tracked live within a region of interest (Figure 1C) and brightfield videos of the entire lymphatic segment were recorded for further analysis. Two-dimensional maps from outside diameter line-scans (STMs) were generated (Figure 1D). These maps

allowed determination of vessel diameter changes as a function of pressure along the entire lymphatic segment under study (i.e. in both valve and non-valve areas).

Next, changes in vessel diameter were measured while the function and competence of each lymphatic valve was tested by subjecting the vessel to an adverse increasing (ramp-wise) pressure (i.e. P_{in}=0.5 cmH_2O and P_{out}=[0.5,10] cmH_2O), Figure 2A. In fully competent (i.e. tight) valves, increasing the output pressure caused the valves to close at low P_{out} values (0.6-0.7 cmH_2O) after which the output side of the lymphatic segment subsequently distended (Figure 2B). Importantly, even though the closed valve successfully prevented pressure back-leak into the input side (i.e. servo-null pressure remained at ~0.5 cmH_2O), the distention of the valve sinus area resulted in a non-pressure driven increase in vessel diameter in the upstream region immediately adjacent to the base of the valve (Figure 2B,D-E). However, apart from that area, the change in diameter on the input side of the valve was negligible (Figure 2C), as evident by the blue colors throughout the entire output pressure ramp (Figure 2E). In contrast, increasing the output pressure (Figure 3A) in lymphatic segments containing a very leaky valve resulted in back-leak of pressure into the input side (i.e. servo-null pressure in the input side read ~5.1 cmH_2O when output pressure reached 10 cmH_2O) with concomitant enlargement of the vessel diameter throughout the entire segment (Figure 3B-E). As anticipated, away from the valve area, the distention of the vessel diameter on the input side depended on the degree of dysfunction of the valve and the associated pressure back-leak (Figure 3B,C). Therefore, we developed a simplified method to quantify the back-leak of pressure based on diameter changes upstream from a tested valve. It is important to note that the 2-dimensional STMs shown in Figures 1-3 are not necessary for calculation of back-leak of pressure using the method described in the following section; however, they help identify the optimal location along the lymphatic vessel to record changes in diameter. The STMs in Figures 2-3 show that diameter measurement at the input side of the vessel (upstream from the valve) and away from the valve sinus provides a reliable indicator of pressure back-leak.

Assessment of Lymphatic Valve Back-leak Using Pressure-Driven Changes in Diameter

To quantify the degree of pressure back-leak from the diameter change, a servo-null micropipette was positioned in the lumen of the input side, upstream from the valve (Figure 4A), P_{in} and P_{out} were set to 0.5 cmH_2O and vessel diameter was allowed to reach a steady level. As shown in Figure 4A, outside diameter was tracked on the input side, near the input cannulating pipette and away from the valve area. Calibration curves were obtained by simultaneously increasing both input and output pressure in a ramp-wise manner from 0.5 to 10 cmH_2O (Figure 4B) while outside diameter was recorded and expressed as change in outside diameter (Figure 4C). In order to subsequently assess the back-leak of pressure through the valve undergoing testing, back-leak test curves were obtained by increasing P_{out} in a ramp-wise manner from 0.5 to 10 cmH_2O while keeping P_{in} constant at 0.5 cmH_2O (Figure 4E). Under these conditions, intraluminal pressure measured by the servo-null micropipette (Figure 4D) and outside diameter were recorded at the input side as a function of the increasing output pressure. It is critical that both calibration and back-leak curves are obtained from diameter tracking at the same position along a given lymphatic vessel. We decided to use the calculated change in diameter as it was a better indicator of pressure change (Figure 4F). Calibration and back-leak test curves were repeated 3 times each in an alternating manner. In order to minimize hysteresis in the pressure-diameter curve, prior to each pressure ramp (either calibration or back-leak test), the vessel wall was unloaded by briefly setting intraluminal pressure to 0 cmH_2O for about 10 seconds, and then diameter was allowed to equilibrate at 0.5 cmH_2O for about 2-3 minutes (until diameter reached a steady level). Back-leak of pressure was calculated from the change in diameter as follows: 1) from the back-leak test pressure ramp (Figure 4E), for a given/selected output pressure value, its corresponding time label was identified. In the example shown in Figure 4, back-

leak of pressure is calculated when output pressure was equal to 5 cmH_2O (Figure 4E); 2) the time label associated with the specific testing pressure (i.e. ~0.7 min) was mapped onto the change in the outside diameter curve (Figure 4F); 3) subsequently, that change in outside diameter value (i.e. 7.89 μm) was compared to the calibration trace of the change in diameter (Figure 4C); 5) and finally, this change in diameter value was mapped onto its corresponding calibration pressure ramp (Figure 4B) to identify the intraluminal pressure level that would cause such change in outside diameter. In this example, the diameter-based method allowed us to determine a diameter-based pressure of 1.09 cmH_2O (i.e. pressure back-leak equals 0.59 cmH_2O – pressure difference from baseline), which is very comparable with the actual pressure measurement from the servo-null recording (1.06 cmH_2O, from Figure 4D). This method and the specific experimental example shown in Figure 4 is also visually described in Supplemental Video 1 (back-leak test) and Supplemental Video 2 (calibration curve).

Back-leak Pressure Measurements on Mesenteric Lymphatic Valves: Endothelium-Specific Deletion of Connexin43 in Connexin37 Globally-Deficient Mice Results in Full Regression of Lymphatic Valves

In the mouse, mesenteric valves are widely used in studies assessing the role of genes controlling valve development and valve maintenance. This is in part due to the extensive number of lymphatic vessels and lymphatic valves that are present in the mesentery and the ease of imaging these valves. However, determining the degree of competency of lymphatic valves requires graded measurement of valve function, which remains undetermined for mesenteric valves. Therefore, we assessed the degree of pressure back-leak using isolated mesenteric lymphatic valves from *WT* (*C57BL/6J* control, fully-functional valves); and, *Ub-CreER^{T2};Rasa1$^{fx/fx}$*, *Foxc2$^{Cre/+}$*, *Lyve1-Cre;Cx43$^{fx/fx}$*, and *Prox1-CreER^{T2};Cx43$^{fx/fx}$;Cx37$^{-/-}$* mice. These genes (i.e. *Rasa1*, *Foxc2*, *Cx43*, and *Cx37*) have previously been linked to lymphatic valve dysfunction associated with immaturely formed or regressed valve leaflets. In order to validate our diameter-based method, simultaneous measurements were performed using a servo-null micropressure system and compared the results with diameter-based extrapolation. As in the previous section, 3 sets of calibration and back-leak test curves were recorded, with each value in each back-leak test curve compared to all calibration curves. Pressure back-leak was determined when valves were challenged with an adverse (output) pressure equal to 5 cmH_2O, while input pressure was maintained at 0.5 cmH_2O, and calculated back-leak was compared to the corresponding servo-null measurement (Figure 5A,B). Importantly, measurements of pressure back-leak using both servo-null and the diameter-based method were statistically comparable (i.e. data is linearly correlated, Pearson's correlation coefficient r=0.9839, $p<0.05$). The fully-functional (non-leaky) and mildly leaky valves are located in the bottom left corner in Figure5A (inside dashed box). A zoomed-in view of these values is shown in Figure 5B. In Figure 5A, the dotted straight line represents the ideal scenario (i.e. slope = 1), where both our diameter-based method and the servo-null microsystem would provide identical pressure back-leak values. In Figures 5A,B, data are shown as the mean ± standard-deviation for each experiment (a total of "*n*" experiments were performed for each group); and Figure 5E shows all individual data-points for each group.

Our data from WT and *Rasa1*-deficient mesenteric valves (Figure 5A,B,E) confirm the findings of our previous studies in popliteal lymphatics: essentially no back-leak (i.e. normal function) of WT valves and ~50% of *Rasa1*-deficient valves with nearly complete back-leak (Lapinski *et al.*, 2017). Likewise, lymphatic endothelium-specific *Cx43*-deficient (i.e. *Lyve1-Cre;Cx43$^{fx/fx}$*) valves showed a wide range of phenotypes from tight to intermediate back-leak (Figure 5A,B,E), also in accord with previous findings in popliteal lymphatic valves (Munger *et al.*, 2017). Data from two new genotypes of mice for which back-leak has not previously been assessed are also reported in Figure 5: *Foxc2$^{Cre/+}$* valves, which are haplodeficient in *Foxc2,* and *Prox1-CreER^{T2};Cx43$^{fx/fx}$;Cx37$^{-/-}$* valves deficient in both Cx43 (postnatal deletion)

and Cx37, the two most widely expressed connexin isoforms in lymphatic endothelial cells (LECs) (Kanady *et al.*, 2011; Meens *et al.*, 2014). In a previous study, we reported that complete knockout of *Foxc2* from LECs results in a high percentage of completely incompetent valves with severely shortened leaflets (Sabine *et al.*, 2015); it is therefore somewhat surprising that *Foxc2* haplodeficient (*Foxc2*$^{Cre/+}$) valves do not show an intermediate back-leak phenotype but rather are almost normal (Figure 5A,B,E), at least when valves are challenged with an outflow pressure of 5 cmH_2O. This suggests that complete or nearly complete deletion of *Foxc2* is required to produce a severe valve defect. In contrast, postnatal, endothelium-specific deletion of Cx43 (using the Prox1-CreER^{T2} driver) in Cx37-globally-deficient (Cx37$^{-/-}$) mice produced severe valve regression, up to the point that long segments (~5 mm) of mesenteric lymphatic vessels could be observed with apparent sinuses but no valves; such segments otherwise should have contained 3-5 valves. In other cases, shorter segments like the ones studied here had varying degrees of leaflet regression, from partial leaflets to short stubs where leaflets once were present (Figure 5D), in contrast to fully-formed, competent valves in WT vessels (Figure 5C). Since these vessels were studied only 5-7 days after the mouse was induced with tamoxifen (i.e. following the end of a week-long induction period), this is the most rapid instance of valve regression described so far; faster than LEC-specific *Foxc2*-deficient (*Foxc2*^{LECKO}) mice in which some valves remained after 4 weeks (Sabine *et al.*, 2015) and faster than *Rasa1*^{LECKO} mice in which some valves remained after 5 months (Lapinski *et al.*, 2017).

Accuracy and Precision of the Diameter-Based Back-Leak Measurement

We then evaluated the accuracy and precision of the diameter-based method for calculating pressure back-leak. Since this method relies on the accurate detection of changes in diameter driven by changes in intraluminal pressure, we first determined and compared the cross-sectional distensibility of each lymphatic segment included in this study. The cross-sectional distensibility is a parameter that measures the degree of diameter change due to a given change in intraluminal pressure. Similar to blood vessels, lymphatics from different anatomical regions display different mechanical characteristics. When examining the cross-sectional distensibility of mesenteric lymphatics from the different groups included here, we found that lymphatic vessels from Foxc2$^{Cre/+}$ mice were significantly more distensible than vessels from all the other groups (Figure 6A). We then proceeded to calculate the accuracy and the precision of our diameter-based measurements of pressure back-leak. The precision, indicative of measurement reproducibility, is directly associated with the standard deviation of a given set of collected repeated, consecutive measurements on the same sample. Our analysis shows that this simplified diameter-based method is both highly accurate and precise as evident by the respective low error and standard deviation values (Figure 6B,C). While there are no-significant differences in error and standard deviation between groups, there appeared to be a correlation between cross-sectional distensibility and accuracy; this is indicated by the higher distensibility and lower error values (higher accuracy) obtained for vessels from Foxc2$^{Cre/+}$ mice (Figure 6A,B). In general, lymphatic vessels from the various strains displayed higher cross-sectional distensibility in the range of pressure from 1 to 3 cmH_2O (Figure 6A). This becomes highly important in vessels containing incompetent valves (e.g. lymphatic valves from *Ub-CreER*^{T2}*;Rasa1*$^{fx/fx}$, *Lyve1-Cre;Cx43*$^{fx/fx}$, and *Prox1-CreER*^{T2}*;Cx43*$^{fx/fx}$*;Cx37*$^{-/-}$ mice), where the pressure back-leak ≥ 3 cmH_2O, and consequently the distensibility is minimal, thereby limiting accurate and precise measurement of diameter changes. While not significantly different, there was a tendency for precision to decrease (i.e., higher standard-deviation values) as pressure back-leak increased (Figure 6C). Finally, the percent accuracy as a function of the precision (standard-deviation) was calculated (Figure 6D). Here, clustering of data-points in the upper-left corner is another indicator of high accuracy (i.e. 85% of the measurements display an 80% or higher percent accuracy) and high precision (i.e. 80% of the measurements fall within a standard deviation of 0.2 cmH_2O or lower) associated with the measurement of pressure back-leak using our diameter-based method.

Discussion

Abnormal fluid accumulation associated with lymphatic dysfunction can result from impaired contractility of collecting lymphatics and/or incompetent lymphatic valves that cannot cope with the chronic adverse hydrostatic pressure load imposed by gravitational forces (Olszewski & Engeset, 1980; Olszewski, 2002; Modi *et al.*, 2007; Stanton *et al.*, 2009; Ferrell *et al.*, 2010; Kanady *et al.*, 2011; Ostergaard *et al.*, 2011; Finegold *et al.*, 2012; Sabine *et al.*, 2012; Brice *et al.*, 2013; Geng *et al.*, 2016). At present, the single technique capable of quantifying back-leak through intact isolated lymphatic valves uses the servo-null micropressure system (Davis *et al.*, 2011a; Lapinski *et al.*, 2017), which: 1) is difficult to learn, 2) requires instrumentation that is no longer available commercially; 3) involves the insertion of a servo-null pipette that can be easily plugged if not inserted through a pre-made hole in the vessel wall made with a pilot pipette; and 4) requires a 45^{o}-angle micromanipulator. Here we have developed, tested, and validated a simplified method that utilizes the pressure-driven changes in vessel passive diameter to calculate pressure back-leak through a lymphatic valve being studied using pressure myography. Outside diameter recording was used simultaneously with servo-null micropressure measurement to test and validate our method; however, we also confirmed that inner diameter tracking gave comparable results. We used outside over inner diameter tracking because outside diameter tracking can easily be achieved using various already available, open-source tools: VasoTracker (Lawton *et al.*, 2019), ImageJ, etc. In addition to reporting novel findings on valve function/dysfunction in lymphatic valves from *Foxc2*$^{Cre/+}$ and *Prox1-CreER*^{T2}*;Cx43*$^{fx/fx}$*;Cx37*$^{-/-}$ mice, the significance of this work comes in making available a more accessible technique for quantitative measurement of lymphatic valve function. This novel method was tested in a large set of mesenteric lymphatic valves displaying a wide range of dysfunction. However, this method could be adapted easily, with minor modifications, to study lymphatic valves from different anatomical regions or from other species, including humans. Our method should also be applicable to studies of venous valve function.

Mesenteric valves have been the target for several developmental studies to assess the role of critical transcriptional factors that control valve development and maintenance. Such studies typically rely on imaging techniques to quantify valve density within the lymphatic vasculature and/or identify abnormal looking valves. Conclusions about abnormal valve appearance can be complicated by valve orientation and, in mature animals, by the presence of overlying connective and adipose tissue; in any case, they do not assess actual valve function.

Our method is capable of quantitatively assessing lymphatic valve competency (i.e. pressure back-leak) with high accuracy and high precision. As our method relies on the ability to measure changes in vessel wall diameter that result from changes in intraluminal pressure, the distensibility of a vessel will determine the working range and accuracy of back-leak measurements. This is important, because lymphatic vessels from different beds display different degrees of distensibility; and consequently, the accuracy of this method may be different for lymphatic vessels from different areas of the body. In general, lymphatics are more distensible in the lower range of pressure (i.e. 1-3 cmH_2O). This is directly correlated with the degree of accuracy of our diameter-based method to assess lymphatic valve function such that measurements are accurate in the low range of pressures but become noisy and less accurate at higher pressures. The impact of distensibility on the working range, accuracy, and precision of the diameter-based measurement of pressure back-leak should be taken into consideration when comparing valve function in vessels from mice with different genotypes and/or phenotypes in which distensibility could change along with valve function. For example, arterial/arteriolar distensibility has been reported to be altered in obesity, diabetes, and hypertension (Reneman & Hoeks, 1995; Van Bortel *et al.*, 1995;

Tentolouris *et al.*, 2003; Bender *et al.*, 2015; Foote *et al.*, 2016; Ljunggren *et al.*, 2016); and lymphatic vessel distensibility (although not reported under those conditions) could change as well. Such changes could easily be accounted for in valve function studies by measuring vessel distensibility curves (obtained during valve function tests) for the various genotypes.

A requirement of our method and the servo-null method to detect back-leak is having an inflow pipette with a relatively high hydraulic resistance, allowing pressure to rise between the valve and the tip of the inflow pipette, in which pressure is held at 0.5 cmH_2O. Pipettes with different resistances would lead to differences in the determination of the amount of back-leak for a given valve. For this reason, we were careful, as in previous studies, to use the same pairs of inflow and outflow pipettes for all experiments, i.e. for all 41 valve tests in the 5 different genotypes of mice. This limitation would need to be taken into consideration in future studies investigating venous valves or larger lymphatic vessels, e.g. from humans.

We validated our diameter-based method by assessing the function of a large set of mesenteric valves displaying a wide range of competency, i.e. normal, fully-competent valves from *C57BL/6J* mice to varying degrees of leaky, incompetent valves from *Ub-CreER^{T2};Rasa1$^{fx/fx}$*, *Foxc2$^{Cre/+}$*, *Lyve1-Cre;Cx43$^{fx/fx}$*, and *Prox1-CreER^{T2};Cx43$^{fx/fx}$;Cx37$^{-/-}$* mice. Here we showed that haplodeficiency in *Foxc2* (*Foxc2$^{Cre/+}$*) does not seem to be sufficient to cause significant valve dysfunction compared to when *Foxc2* is completely deleted from LECs. We also showed that postnatal endothelial-specific deletion of Cx43 in Cx37$^{-/-}$ mice resulted in rapid (5-7 days post induction) regression of valve leaflets and severe valve dysfunction. A regression of lymphatic valve leaflets this rapid has not been reported previously. Our present work did not include a survival study; however, a small group (~4 mice) of *Prox1-CreER^{T2};Cx43$^{fx/fx}$;Cx37$^{-/-}$* mice died 2-3 weeks after Cx43-deletion was induced via tamoxifen feeding. In a few cases, even after only 7 days post-induction, we observed bloody mesenteric lymphatic nodes and blood-filled mesenteric lymphatic vessels. This is important because, global, embryonic deletion of both Cx43 and Cx37 in the mouse prevents normal lymphatic valve development. Cx43$^{-/-}$;Cx37$^{-/-}$ embryos are not viable and display blood-filled lymphatic vasculature and severe edema (Kanady *et al.*, 2011); however, the end cause of death may also be associated with developmental cardiac abnormalities related to the global deletion of Cx43 (Reaume *et al.*, 1995). Therefore, our findings show for the first time, that in mature/adult mice, both Cx43 and Cx37 play a critical role in lymphatic valve maintenance; and sudden deletion of endothelial-Cx43 in global Cx37-deficient mice causes full regression of lymphatic valve leaflets and lymphatic valve incompetence.

ADITIONAL INFORMATION

Competing Interests

The authors have no conflicting interests to declare.

Funding

This work was supported by NIH grants K99-HL141143 to JAC-G, R01-HL120867 to MJD, and R01-HL120888 to PDK.

Acknowledgements

The authors are grateful for the expert assistance of Min Li with mice breeding and the technical help of Shan-Yu Ho and Peichun Gui.

References

Bender SB, Castorena-Gonzalez JA, Garro M, Reyes-Aldasoro CC, Sowers JR, DeMarco VG & Martinez-Lemus LA. (2015). Regional variation in arterial stiffening and dysfunction in Western diet-induced obesity. *Am J Physiol Heart Circ Physiol* **309,** H574-582.

Blatter C, Meijer EFJ, Padera TP & Vakoc BJ. (2018). Simultaneous measurements of lymphatic vessel contraction, flow and valve dynamics in multiple lymphangions using optical coherence tomography. *J Biophotonics* **11,** e201700017.

Brice G, Ostergaard P, Jeffery S, Gordon K, Mortimer PS & Mansour S. (2013). A novel mutation in GJA1 causing oculodentodigital syndrome and primary lymphoedema in a three generation family. *Clin Genet* **84,** 378-381.

Castorena-Gonzalez JA, Scallan JP & Davis MJ. (2018a). Methods for Assessing the Contractile Function of Mouse Lymphatic Vessels Ex Vivo. *Methods Mol Biol* **1846,** 229-248.

Castorena-Gonzalez JA, Zawieja SD, Li M, Srinivasan RS, Simon AM, de Wit C, de la Torre R, Martinez-Lemus LA, Hennig GW & Davis MJ. (2018b). Mechanisms of Connexin-Related Lymphedema. *Circ Res* **123,** 964-985.

Cha B, Geng X, Mahamud MR, Zhang JY, Chen L, Kim W, Jho EH, Kim Y, Choi D, Dixon JB, Chen H, Hong YK, Olson L, Kim TH, Merrill BJ, Davis MJ & Srinivasan RS. (2018). Complementary Wnt Sources Regulate Lymphatic Vascular Development via PROX1-Dependent Wnt/beta-Catenin Signaling. *Cell Rep* **25,** 571-584 e575.

Davis MJ, Rahbar E, Gashev AA, Zawieja DC & Moore JE. (2011a). Determinants of valve gating in collecting lymphatic vessels from rat mesentery. *American Journal of Physiology (Heart and Circulatory Physiology)* **301,** H48-H60.

Davis MJ, Rahbar E, Gashev AA, Zawieja DC & Moore JE, Jr. (2011b). Determinants of valve gating in collecting lymphatic vessels from rat mesentery. *Am J Physiol Heart Circ Physiol* **301,** H48-60.

Davis MJ, Zawieja DC & Gashev AA. (2006). Automated measurement of diameter and contraction waves of cannulated lymphatic microvessels. *Lymphat Res Biol* **4,** 3-10.

Ferrell RE, Baty CJ, Kimak MA, Karlsson JM, Lawrence EC, Franke-Snyder M, Meriney SD, Feingold E & Finegold DN. (2010). GJC2 missense mutations cause human lymphedema. *Am J Hum Genet* **86,** 943-948.

Finegold DN, Baty CJ, Knickelbein KZ, Perschke S, Noon SE, Campbell D, Karlsson JM, Huang D, Kimak MA, Lawrence EC, Feingold E, Meriney SD, Brufsky AM & Ferrell RE. (2012). Connexin 47 mutations increase risk for secondary lymphedema following breast cancer treatment. *Clin Cancer Res* **18,** 2382-2390.

Foote CA, Castorena-Gonzalez JA, Ramirez-Perez FI, Jia G, Hill MA, Reyes-Aldasoro CC, Sowers JR & Martinez-Lemus LA. (2016). Arterial Stiffening in Western Diet-Fed Mice Is Associated with Increased Vascular Elastin, Transforming Growth Factor-beta, and Plasma Neuraminidase. *Front Physiol* **7,** 285.

Geng X, Cha B, Mahamud MR, Lim KC, Silasi-Mansat R, Uddin MK, Miura N, Xia L, Simon AM, Engel JD, Chen H, Lupu F & Srinivasan RS. (2016). Multiple mouse models of primary lymphedema exhibit distinct defects in lymphovenous valve development. *Dev Biol* **409,** 218-233.

Hargens AR & Zweifach BW. (1976). Transport between blood and peripheral lymph in intestine. *Microvascular Research* **11,** 89-101.

Hennig GW. (2016). Spatio-Temporal Mapping and the Enteric Nervous System. *Adv Exp Med Biol* **891,** 31-42.

Hennig GW, Gould TW, Koh SD, Corrigan RD, Heredia DJ, Shonnard MC & Smith TK. (2015). Use of Genetically Encoded Calcium Indicators (GECIs) Combined with Advanced Motion Tracking Techniques to Examine the Behavior of Neurons and Glia in the Enteric Nervous System of the Intact Murine Colon. *Front Cell Neurosci* **9,** 436.

Hennig GW, Spencer NJ, Jokela-Willis S, Bayguinov PO, Lee HT, Ritchie LA, Ward SM, Smith TK & Sanders KM. (2010). ICC-MY coordinate smooth muscle electrical and mechanical activity in the murine small intestine. *Neurogastroenterol Motil* **22,** e138-151.

Kanady JD, Dellinger MT, Munger SJ, Witte MH & Simon AM. (2011). Connexin37 and Connexin43 deficiencies in mice disrupt lymphatic valve development and result in lymphatic disorders including lymphedema and chylothorax. *Dev Biol* **354,** 253-266.

Karkkainen MJ, Ferrell RE, Lawrence EC, Kimak MA, Levinson KL, McTigue MA, Alitalo K & Finegold DN. (2000). Missense mutations interfere with VEGFR-3 signalling in primary lymphoedema. *Nat Genet* **25,** 153-159.

Lapinski PE, Lubeck BA, Chen D, Doosti A, Zawieja SD, Davis MJ & King PD. (2017). RASA1 regulates the function of lymphatic vessel valves in mice. *J Clin Invest* **127,** 2569-2585.

Lawton PF, Lee MD, Saunter CD, Girkin JM, McCarron JG & Wilson C. (2019). VasoTracker, a Low-Cost and Open Source Pressure Myograph System for Vascular Physiology. *Front Physiol* **10,** 99.

Liao Y, Day KH, Damon DN & Duling BR. (2001). Endothelial cell-specific knockout of connexin 43 causes hypotension and bradycardia in mice. *Proc Natl Acad Sci U S A* **98,** 9989-9994.

Ljunggren P, Maahs DM, Johansson P, Ludvigsson J, Pyle L, Sippl R, Wadwa RP & Snell-Bergeon J. (2016). Reduced brachial artery distensibility in patients with type 1 diabetes. *J Diabetes Complications* **30,** 893-897.

Meens MJ, Sabine A, Petrova TV & Kwak BR. (2014). Connexins in lymphatic vessel physiology and disease. *FEBS Lett* **588,** 1271-1277.

Modi S, Stanton AW, Svensson WE, Peters AM, Mortimer PS & Levick JR. (2007). Human lymphatic pumping measured in healthy and lymphoedematous arms by lymphatic congestion lymphoscintigraphy. *J Physiol* **583,** 271-285.

Munger SJ, Davis MJ & Simon AM. (2017). Defective lymphatic valve development and chylothorax in mice with a lymphatic-specific deletion of Connexin43. *Dev Biol* **421,** 204-218.

Nonomura K, Lukacs V, Sweet DT, Goddard LM, Kanie A, Whitwam T, Ranade SS, Fujimori T, Kahn ML & Patapoutian A. (2018). Mechanically activated ion channel PIEZO1 is required for lymphatic valve formation. *Proc Natl Acad Sci U S A* **115,** 12817-12822.

Olszewski WL. (2002). Contractility patterns of normal and pathologically changed human lymphatics. *Ann N Y Acad Sci* **979,** 52-63; discussion 76-59.

Olszewski WL & Engeset A. (1980). Intrinsic contractility of prenodal lymph vessels and lymph flow in human leg. *Am J Physiol* **239,** H775-783.

Ostergaard P, Simpson MA, Brice G, Mansour S, Connell FC, Onoufriadis A, Child AH, Hwang J, Kalidas K, Mortimer PS, Trembath R & Jeffery S. (2011). Rapid identification of mutations in GJC2 in primary lymphoedema using whole exome sequencing combined with linkage analysis with delineation of the phenotype. *J Med Genet* **48,** 251-255.

Reaume AG, de Sousa PA, Kulkarni S, Langille BL, Zhu D, Davies TC, Juneja SC, Kidder GM & Rossant J. (1995). Cardiac malformation in neonatal mice lacking connexin43. *Science* **267,** 1831-1834.

Reneman RS & Hoeks AP. (1995). Arterial distensibility and compliance in hypertension. *Neth J Med* **47,** 152-161.

Sabine A, Agalarov Y, Maby-El Hajjami H, Jaquet M, Hagerling R, Pollmann C, Bebber D, Pfenniger A, Miura N, Dormond O, Calmes JM, Adams RH, Makinen T, Kiefer F, Kwak BR & Petrova TV. (2012). Mechanotransduction, PROX1, and FOXC2

cooperate to control connexin37 and calcineurin during lymphatic-valve formation. *Dev Cell* **22,** 430-445.

Sabine A, Bovay E, Demir CS, Kimura W, Jaquet M, Agalarov Y, Zangger N, Scallan JP, Graber W, Gulpinar E, Kwak BR, Makinen T, Martinez-Corral I, Ortega S, Delorenzi M, Kiefer F, Davis MJ, Djonov V, Miura N & Petrova TV. (2015). FOXC2 and fluid shear stress stabilize postnatal lymphatic vasculature. *J Clin Invest* **125,** 3861-3877.

Sabine A, Davis MJ, Bovay E & Petrova TV. (2018). Characterization of Mouse Mesenteric Lymphatic Valve Structure and Function. *Methods Mol Biol* **1846,** 97-129.

Scallan JP & Davis MJ. (2013). Genetic removal of basal nitric oxide enhances contractile activity in isolated murine collecting lymphatic vessels. *J Physiol* **591,** 2139-2156.

Scallan JP, Wolpers JH & Davis MJ. (2013). Constriction of isolated collecting lymphatic vessels in response to acute increases in downstream pressure. *J Physiol* **591,** 443-459.

Scallan JP, Zawieja SD, Castorena-Gonzalez JA & Davis MJ. (2016). Lymphatic pumping: mechanics, mechanisms and malfunction. *J Physiol* **594,** 5749-5768.

Simon AM, Goodenough DA, Li E & Paul DL. (1997). Female infertility in mice lacking connexin 37. *Nature* **385,** 525-529.

Stanton AW, Modi S, Bennett Britton TM, Purushotham AD, Peters AM, Levick JR & Mortimer PS. (2009). Lymphatic drainage in the muscle and subcutis of the arm after breast cancer treatment. *Breast Cancer Res Treat* **117,** 549-557.

Tentolouris N, Liatis S, Moyssakis I, Tsapogas P, Psallas M, Diakoumopoulou E, Voteas V & Katsilambros N. (2003). Aortic distensibility is reduced in subjects with type 2 diabetes and cardiac autonomic neuropathy. *Eur J Clin Invest* **33,** 1075-1083.

Van Bortel LM, Kool MJ, Boudier HA & Struijker Boudier HA. (1995). Effects of antihypertensive agents on local arterial distensibility and compliance. *Hypertension* **26,** 531-534.

Wiederhielm CA, Woodbury JW, Kirk S & Rushmer RF. (1964). Pulsatile pressures in the microcirculation of frog's mesentery. *American Journal of Physiology* **207,** 173-176.

Zawieja SD, Castorena-Gonzalez JA, Dixon B & Davis MJ. (2017). Experimental Models Used to Assess Lymphatic Contractile Function. *Lymphat Res Biol* **15,** 331-342.

Zawieja SD, Castorena-Gonzalez JA, Scallan JP & Davis MJ. (2018). Differences in L-type Ca(2+) channel activity partially underlie the regional dichotomy in pumping behavior

by murine peripheral and visceral lymphatic vessels. *Am J Physiol Heart Circ Physiol* **314,** H991-H1010.

Figure 1. Pressure-driven changes in vessel diameter. A) Isolated, cannulated, and pressurized single-valve mesenteric lymphatic vessel segment from the mouse with independent control of input and output pressures (i.e. P_{in} and P_{out} respectively). B) Double (i.e. input and output) pressure ramp traces. C) Outside diameter (O.D.) as a function of pressure recorded from the single tracking window shown in the top panel. D) Space time map (STM) generated from an outside diameter line scan showing the change in diameter as a function of time (horizontal axis) along the entire lymphatic segment (position is indicated on the vertical axis and it aligns with the vessel image shown on the left side) as pressure increases in a ramp-wise manner (panel B). Outside diameter is encoded in a color-scale as indicated to the right of the heat map. The time (horizontal) axis is matched in panels B-D. Vessel wall diameter changes are determined as a function of pressure by mapping the diameter values in C and D to the pressure ramp values in B.

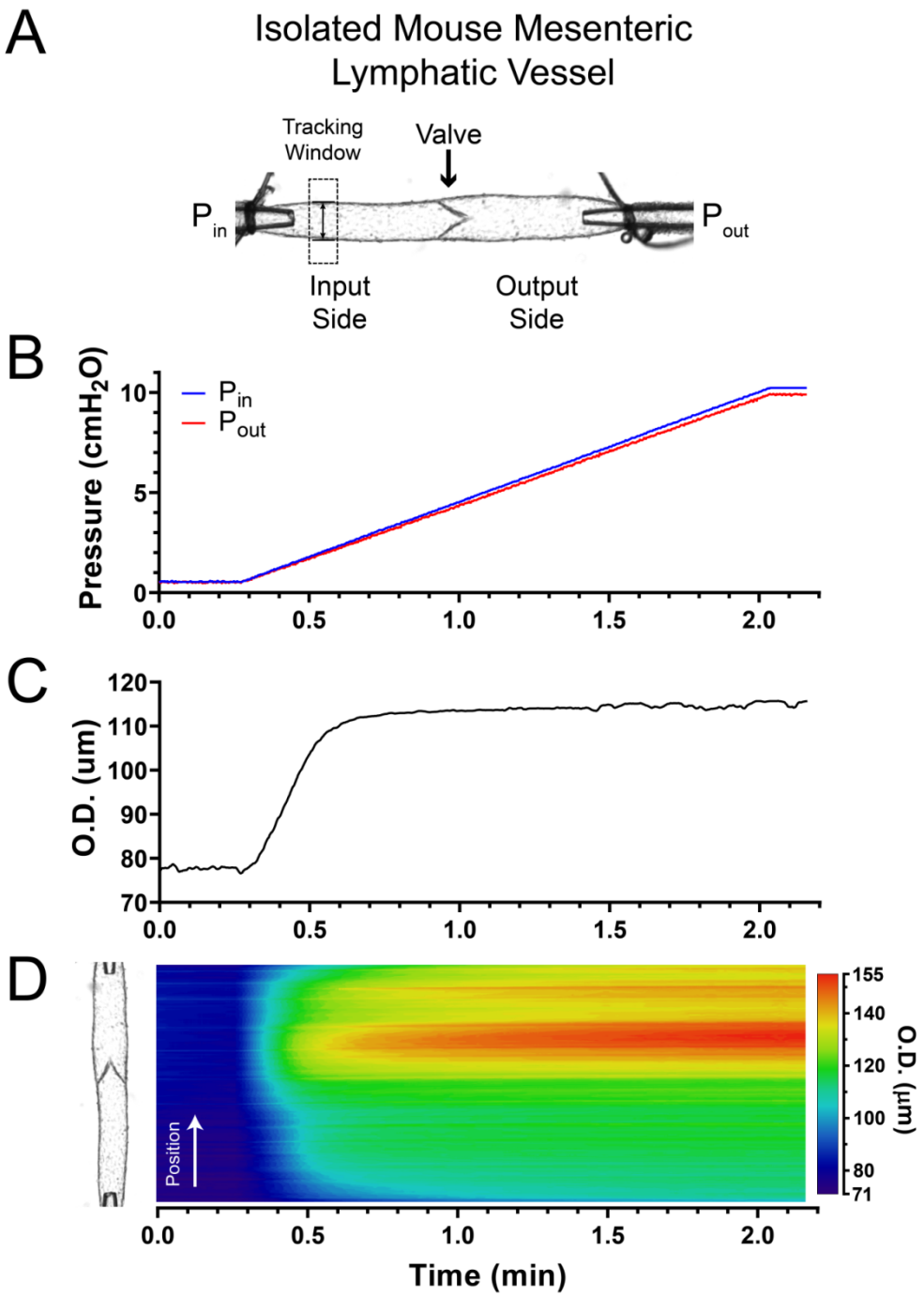

Figure 2. Pressure-driven changes in vessel diameter in a mesenteric lymphatic segment containing a single, fully-competent valve. A) Ramp-wise increase in output pressure (0.5-10 cmH_2O) while input pressure is held constant at 0.5 cmH_2O. B) STM generated from outside diameter tracking (encoded in a color-scale) for a fully-competent, single-valve mesenteric lymphatic segment as a function of time/pressure. Vessel image preparations on both left and right side of the colored STM show the vessel at the initial (P_{in}=P_{out}=0.5 cmH_2O) and final (P_{in}=0.5 cmH_2O and P_{out}=10 cmH_2O) states. C) Outside diameter (O.D.) tracking as a function of time/pressure recorded at a single site upstream from the valve (tracking window shown in panel B); diameter remains significantly unchanged even when the pressure downstream from the valve (i.e. output pressure) reaches 10 cmH_2O. Zoomed-in insert shows an initial distension of the vessel wall at the onset of the pressure ramp and sudden drop in vessel diameter after the lymphatic valve closes as a result of the adverse pressure gradient. D) Image from an actual lymphatic vessel preparation showing a fully-competent (i.e. tight) valve preventing pressure back-leak when output pressure reaches 10 cmH_2O; input pressure remains constant at 0.5 cmH_2O as measured by servo-null micropressure system. E) Same image with outside diameter encoded in a multi-color scale, showing how a fully-competent valve prevents pressure back-leak and results in negligible distention of the lymphatic wall upstream from the valve, while vessel diameter reaches maximum distention downstream from the valve where output pressure has reached 10 cmH_2O.

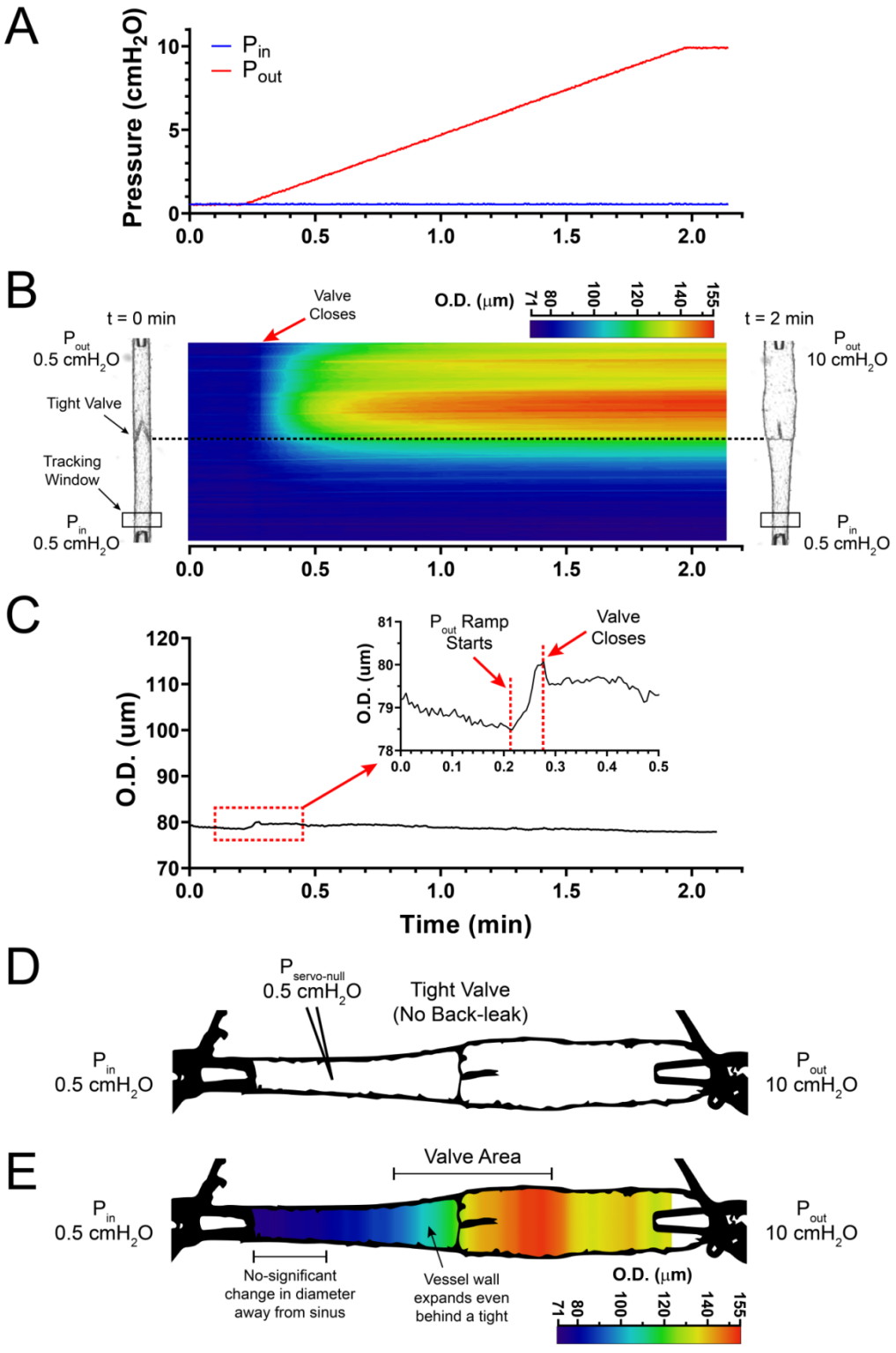

Figure 3. Pressure-driven changes in wall diameter in a mesenteric lymphatic segment containing a single valve displaying a significant degree of dysfunction. A) Ramp-wise increase in output pressure (0.5-10 cmH_2O), with input pressure being held constant at 0.5 cmH_2O. B) STM generated from outside diameter tracking (encoded in a color-scale) as a function of time/pressure for a mesenteric lymphatic segment containing a highly dysfunctional, single valve. Vessel images on the left and right sides of the STM show the vessel at the initial (P_{in}=P_{out}=0.5 cmH_2O) and final pressures, respectively. C) Outside diameter (O.D.) tracking as a function of time/pressure recorded at a single site upstream from the valve (see panel B for location of tracking window). Consistent and significant increase in vessel diameter as pressure downstream from the valve (P_{out}) increases from 0.5 to 10 cmH_2O, resulting in back-leak into the input side. D) Image of a lymphatic vessel preparation with significant pressure back-leak, as evident by vessel wall distention at the input side when output pressure reaches 10 cmH_2O. While input pressure was set to 0.5 cmH_2O actual pressure in the input side reached ~5.1 cmH_2O (determined by servo-null system) as a result of substantial pressure back-leak through the dysfunctional valve. E) Outside diameter encoded in a multi-color scale. Diagram shows how pressure back-leak results in distention of the entire lymphatic segment, which contrasts with distention of the output side with a fully-competent valve.

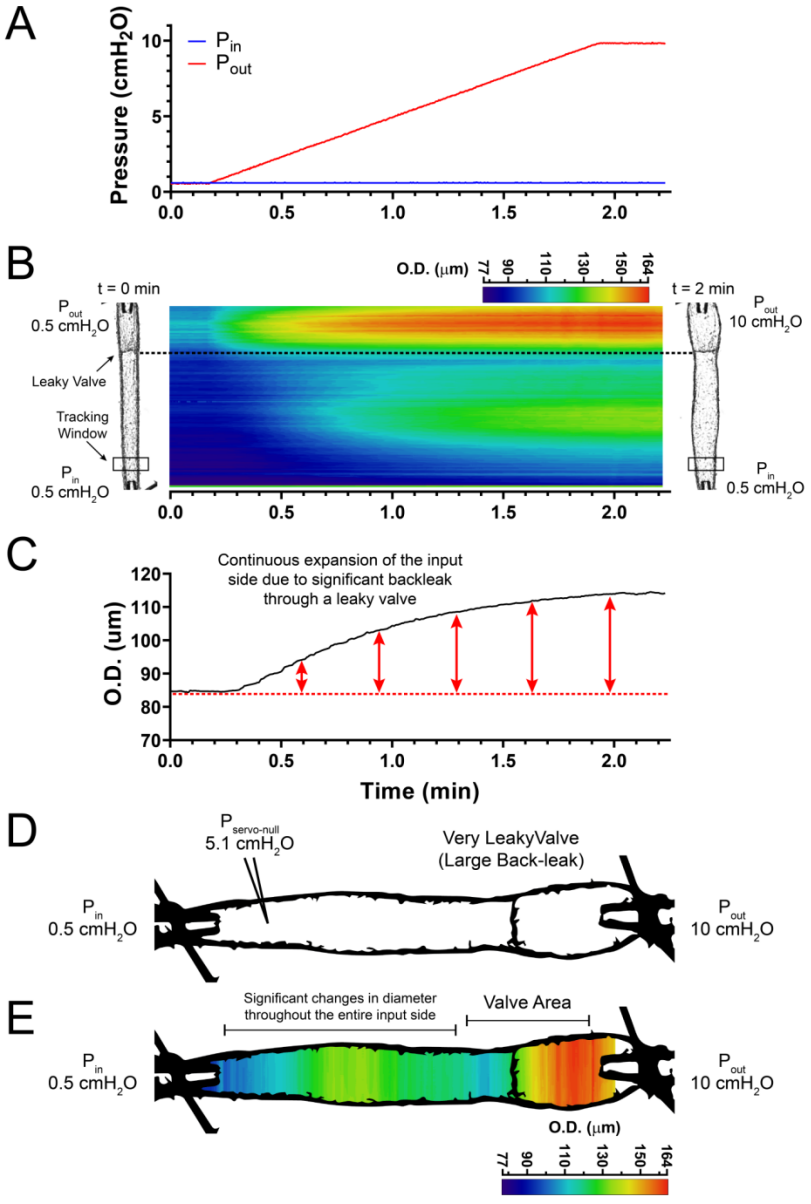

Figure 4. Diameter-based method for extrapolating pressure back-leak through a single, intact valve in an isolated, cannulated, and pressurized lymphatic vessel. A) Single-valve lymphatic segment showing a single-site diameter tracking window and a servo-null glass micropipette to record intraluminal pressure. In this example, this valve displayed an intermediate degree of dysfunction (i.e. partial leak). Servo-null pipette positioned in vessel lumen after micropuncture of the lymphatic wall at the input side near the input pipette. B) Calibration pressure ramp generated by simultaneously increasing both input and output pressure in a ramp-wise manner (0.5 to 10 cmH_2O). C) Trace of the change in outside diameter as a function of time as pressure increases during the calibration pressure ramp (as shown in B). D) Intraluminal pressure, from servo-null micropipette recording, showing increase in intraluminal pressure as output pressure rises (as shown in E) and leaks back into the input side through the partially defective valve. E) Back-leak test pressure ramp in which output pressure is increased in a ramp-wise manner from 0.5-10 cmH_2O, while input pressure is held constant at 0.5 cmH_2O. F) Trace of the change in outside diameter as a function of time and as output pressure is increased. Numbers represent each one of the 4 steps needed for pressure back-leak calculation. Briefly, 1) a test pressure is selected from the back-leak test pressure ramp in E (i.e. 5 cmH_2O); 2) its time label (i.e. ~0.7 min) is mapped to obtain the corresponding change in outside diameter value from the trace in F (i.e. 7.89 µm); 3) this diameter is compared to the calibration change in the diameter trace in C; and finally, the time label associated with this calibration diameter value is mapped onto the calibration pressure ramp, panel B, to determine the intraluminal pressure (i.e. 1.09 cmH_2O) necessary to cause the change in vessel outside diameter in (1).

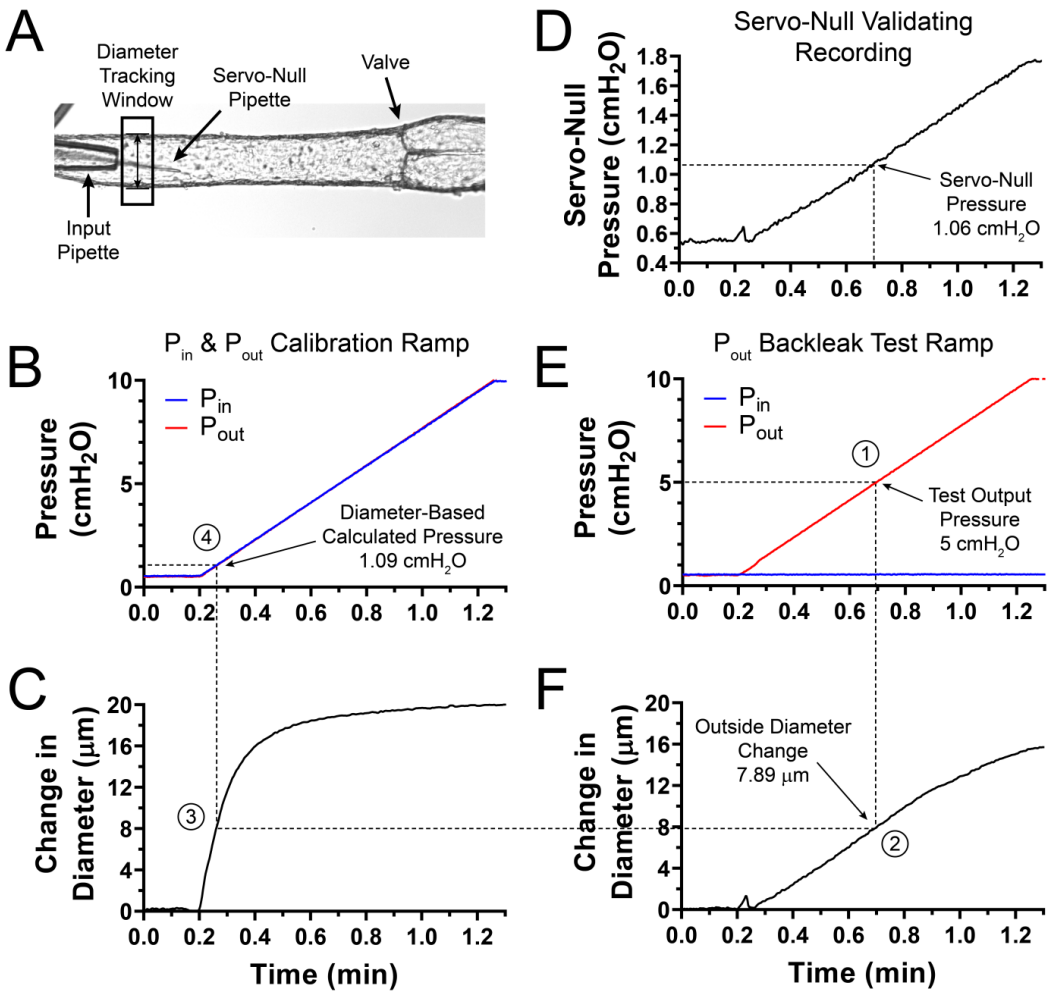

Figure 5. Assessment of pressure back-leak in mesenteric valves displaying various degrees of valve dysfunction. The degree of pressure back-leak was determined in single valves from WT, *Ub-CreER^{T2};Rasa1$^{fx/fx}$*, *Foxc2-Cre*, *Lyve1-Cre;Cx43$^{fx/fx}$*, or *Prox1-CreER^{T2};Cx43$^{fx/fx}$;Cx37$^{-/-}$* mice at 5 cmH_2O adverse (output) pressure. A) Calculated pressure back-leak (measurement referenced to the initial input pressure of 0.5 cmH_2O) using the diameter-based method plotted as a function of the corresponding measured pressure back-leak from a servo-null micropressure recording. Dotted line represents the ideal one-to-one correlation (i.e. slope = 1); servo-null and diameter-based method measurements are linearly correlated with a Pearson's correlation coefficient r=0.9839, $p<0.05$. Values are reported as the mean ± standard-deviation of 9 repeated measurements that result from matching 3 back-leak tests with each of 3 calibration ramps. B) Zoomed-in view of the dotted box shown in panel A (both normal valves and valves displaying a low-to-intermediate degree of dysfunction). Calculation of pressure back-leak using changes in outside diameter upstream from the valve gives accurate and precise values as evident from the corresponding servo-null micropressure measurements. C) Representative image of a mesenteric lymphatic vessel from a WT mouse showing a fully-formed, competent valve. D) Representative image of a mesenteric lymphatic vessel from a *Prox1-CreER^{T2};Cx43$^{fx/fx}$;Cx37$^{-/-}$* mouse showing a severely defective valve where leaflets have almost completely regressed. E) Pressure back-leak measurements per group, with all individual data points shown. * Indicates statistical significance ($p<0.5$) when compared to WT controls using a two-way ANOVA test.

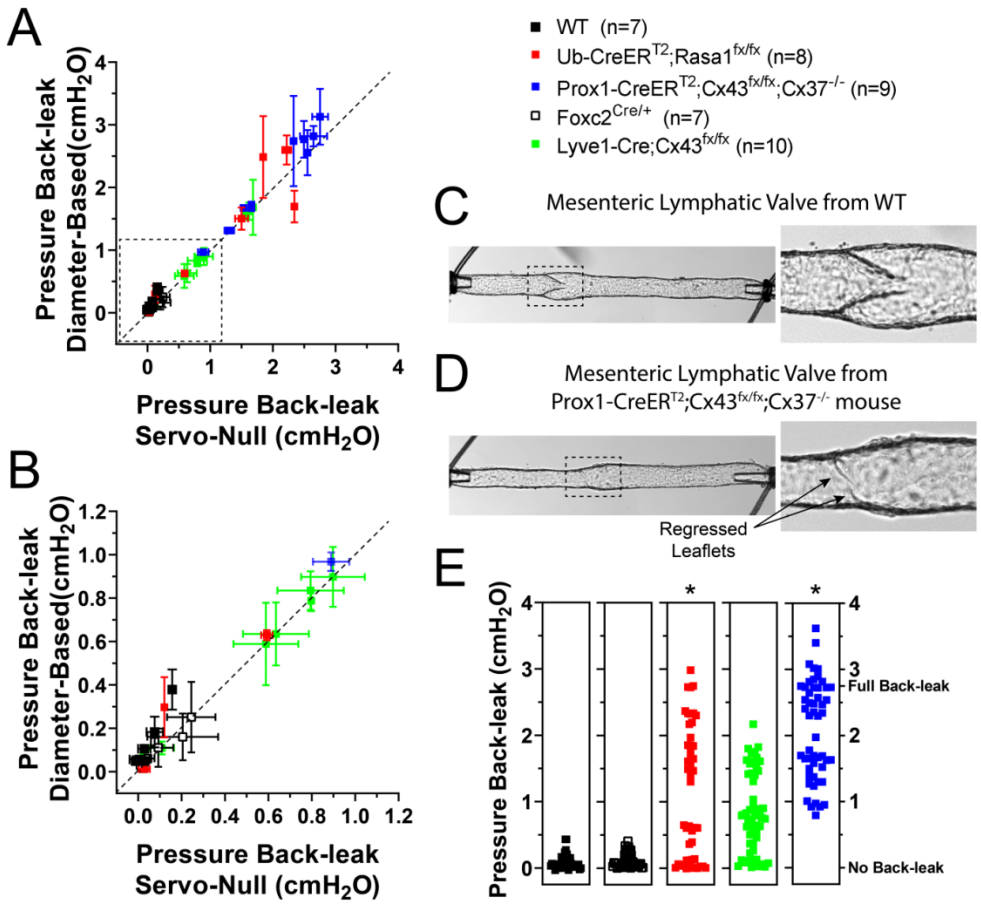

Figure 6. Lymphatic vessel distensibility and assessment of the accuracy and precision of the diameter-based method. A) Group comparison of the cross-sectional distensibility as a function of intraluminal pressure for all of the mesenteric lymphatic vessels included in this study. *Foxc2*-haplodeficient vessels display significantly higher distensibility. In general, all lymphatics are more distensible in the lower range of pressure (<3 cmH_2O). * Indicates statistical significance ($p<0.5$) when compared to WT controls using a two-way ANOVA test. B) Calculated error (absolute difference between the pressure back-leak measurements obtained with a servo-null system and using the diameter-based method). Values measured using a servo-null system are considered the gold-standard/accepted reference. The lower the error, the higher the accuracy of the diameter-based method. C) Precision of the calculated pressure back-leak is directly associated with the standard-deviation resulting from 9 repeated measurements (matching 3 back-leak tests with 3 calibration ramps). In B and C, results are reported as mean ± standard-deviation and box-height is given by the minimum and maximum value observed in each group. Lower precision (larger standard-deviation values) is observed in measurements of pressure back-leak in valves displaying higher degree of dysfunction. D) Percent accuracy plotted as a function of the precision (standard-deviation).

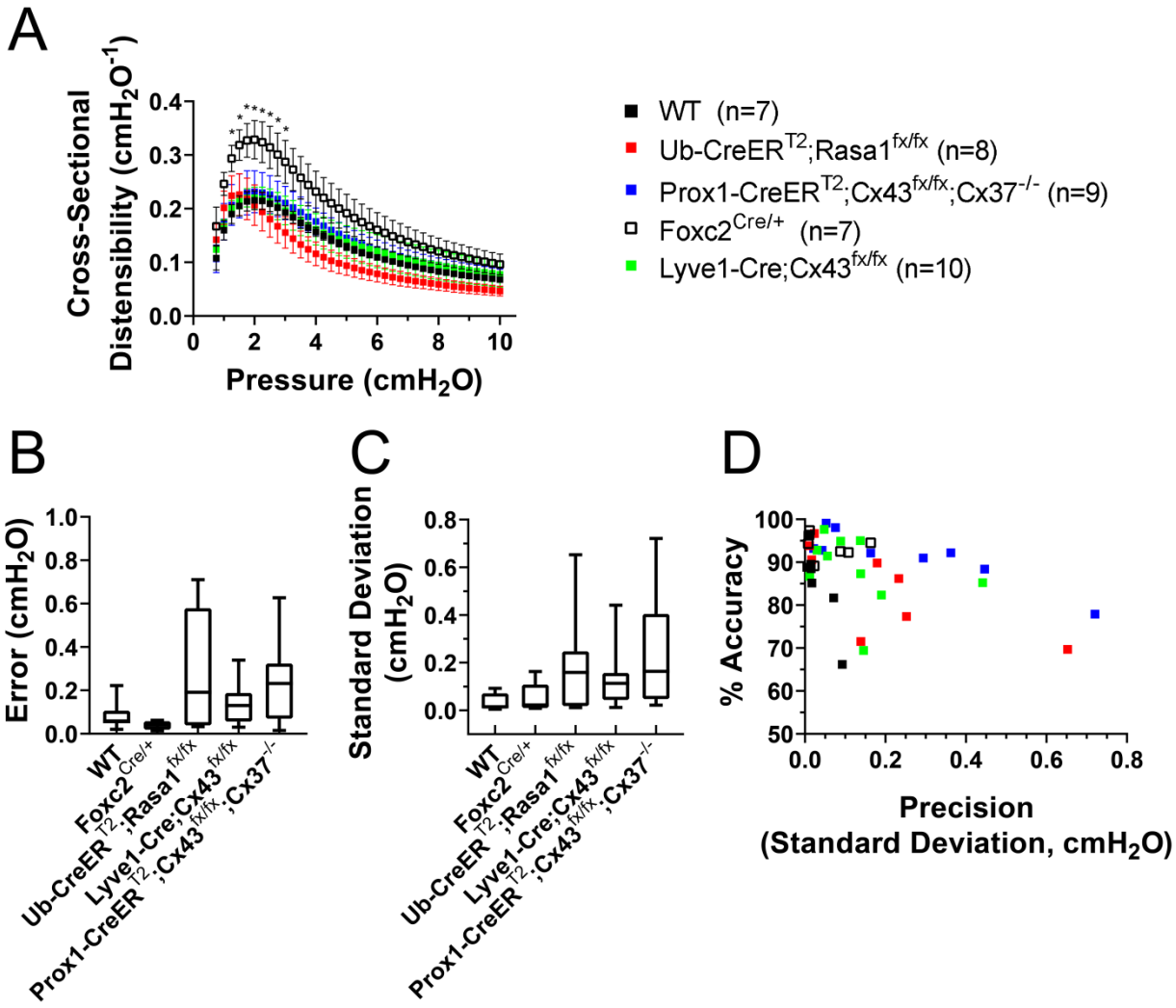

Jorge A. Castorena-Gonzalez earned his BSc and MSc in Physics at the University of Guanajuato in Leon, Mexico. In 2014, Jorge graduated from the PhD program in Bioengineering from the University of Missouri. Dr. Castorena-Gonzalez then worked as a postdoctoral fellow under the mentoring of Dr. Michael J. Davis also at the University of Missouri; there, Jorge acquired a strong training in lymphatic vascular biology. Jorge has recently been promoted to Research Assistant Professor, and his current funded research aims to study lymphatic dysfunction associated with obesity and diabetes, and how it may contribute to the development of cardiovascular diseases.